Biosynthesis, separation and conjugation of gold nanoparticles to doxorubicin for cellular uptake and toxicity

S. Anil Kumar[1,2] Yves-Alain Peter[1] and Jay Nadeau*[2]
[1]Engineering Physics Department, École Polytechnique de Montréal, Montréal, QC Canada H3C 3A7
[2]Department of Biomedical Engineering, McGill University, Montréal, QC Canada H3A 2B4

E-mail: jay.nadeau@mcgill.ca; Phone: 514-398-8372; Fax: 514-398-7461

***Abstract*— Particle shape and size determine the physicochemical and optoelectronic properties of nanoscale materials, including optical absorption, fluorescence, and electric and magnetic moments. It is thus desirable to be able to synthesize and separate various particle shapes and sizes. Biosynthesis using microorganisms has emerged as a more ecologically friendly, simpler, and more reproducible alternative to chemical synthesis of metal and semiconductor nanoparticles, allowing the generation of rare forms such as triangles. Here we show that the plant pathogenic fungus *Helminthosporum solani,* when incubated with an aqueous solution of chloroaurate ions, produces a diverse mixture of extracellular gold nanocrystals in the size range from 2-70 nm. A plurality are polydisperse spheres, but a significant number are homogeneously-sized rods, triangles, pentagons, pyramids, and stars. The particles can be separated according to their size and shape by using a sucrose density gradient using the centrifuge, a novel and facile approach to nanocrystal purification. The smallest separated gold nanoparticles were conjugated to the anti-cancer drug doxorubicin and efficient uptake by and toxicity to HEK293 cells was demonstrated.**

I. Introduction

The size- and shape-dependent properties of semiconductor and metal nanoparticles that arise from quantum confinement create materials qualitatively different from the bulk [7] [1]. Tremendous interest has been generated in the possibility of using these properties for biomedical targeting and labeling applications. The greatest barriers to biological use are issues of particle stability in water [21], toxicity [12], and shape and size control [28]. Colloidal chemical synthesis methods have produced an impressive range of homogeneously size-distributed forms: rods and wires [22, 11], cubes [25], triangles [4], disks [11], and arrows and tetrapods [20]. Challenging forms such as triangular pyramids have also been obtained using shape transformation [14], seeded growth [4], or annealing [5]. However, these methods are complex and often variable from experiment to experiment, and the resulting crystals are often poorly compatible with water and/or biological cells.

An alternative may be sought in biological methods of synthesis [2]. Microbial synthesis of metal [8, 24] and semiconductor [27, 9, 6] nanoparticles has been widely reported, resulting from the microorganisms' intrinsic metal-resistance mechanisms. Advantages of these methods include tightly controlled, highly reproducible syntheses; the generation of water-soluble, biocompatible particles; and the avoidance of toxic surfactants or organic solvents. Disadvantages include lack of control over the resulting shapes and sizes, and often embedding of the particles within the cell matrix, necessitating extraction [26] [8]. A solution to both of these issues is to isolate the enzymes or other proteins responsible for the synthesis and to add them to the reaction mixture under variable conditions, as has been done to create elongated Au nanoparticles with *Escherichia coli* gold-binding enzymes [3] and spherical Au nanoparticles using fungal reductases [15] [16].

Here we use the plant pathogenic fungus, *Helminthosporum solani,* which when seeded with chloroaurate ions ($AuCl_4^-$) generates a mixture of different shapes of gold nanocrystallites in the size

range from 3-70 nm. The particles are extracellular, requiring no purification apart from filtration. We also demonstrate the efficiency of a very simple sucrose density gradient technique to separate the mixture of biosynthesized gold nanoparticles based on their size and shape. Sucrose gradient is a technique commonly used to separate viruses and organelles by ultracentrifugation; it was reported once as a method for separating polymer nanoparticles [23]. In our application, the density of the particles permits separation with low speeds in a tabletop centrifuge. Next, we conjugated the smallest size fractions (~2-5 nm) with an anti-cancerous drug doxorubicin. There are hardly any reports on the conjugation of gold nanoparticles to doxorubicin via EDC mediated cross-linking. We also report on the feasibility of using these conjugates for cancerous cell uptake and toxicity.

2. Experimental methods

Helminthosporum solani was maintained on PDA Petri dishes (potato 20% w/v, dextrose 2% w/v and agar 2% w/v) at 25 ºC. Fermentation was carried out by inoculating a 1 cm diameter mycelium from a 7 day old PDA Petri dish into 100 mL liquid MGYP medium (0.3% w/v malt extract, 1.0% w/v glucose, 0.3% w/v, yeast extract and 0.5% w/v peptone) in a 500 mL Erlenmeyer flask, followed by incubation at 37 ± 1 ºC on a rotary shaker (200 rpm) for 96 h. After the fermentation period, the mycelia were collected by centrifugation (5000 g, 15 ºC, 20 min), washed thoroughly with distilled water under sterile conditions, and 20 g was suspended in 100 mL of 1 mM aqueous $AuCl_4$ solution in a 500 mL Erlenmeyer flask. The culture was then incubated at 37 ± 1 ºC under shaking (200 rpm). Bioreduction was monitored by recording the UV-Vis absorption spectra as a function of time of the reaction mixture. After saturation of the reaction process (found to be 72 h), the reaction mixture was filtered using a sterile 0.2 μM syringe filter.

Separation of the nanoparticles was achieved by creating a discontinuous sucrose density gradient by layering successively dilute sucrose solutions upon one another in a 40 mL centrifuge tube: 6 mL each of 30%, 40%, 50%, 60% and 70% w/v sucrose. The tube was marked in increments of single percentage points within each region. Finally 6 mL of the gold nanoparticles mixture was loaded onto this gradient in ddH2O and centrifuged at 5000 rpm for 30 min in a centrifuge (IEC Centra-8R centrifuge, International Equipment, Company, MA). Fractions (2 mL, representing approximately 3.3% increments) of the gradient were collected using a micropipette and characterized by TEM.

For the UV-Visible spectra of the separated fractions, individual fractions were, dialyzed against Milli Q water and concentrated to half of their volumes using Speed Vac, SC 100 (Savant Instruments, Minnesota, USA) and measured, whereas to get optical color of the separated fractions, the above step is repeated 2-3 times.

The smallest Au nanoparticle fractions (~ 2-5 nm) obtained after sucrose density gradient were functionalized to doxorubicin by using the activator 1-ethyl-3-(3dimethylaminopropyl)-carbodiimide (EDC). The reaction was carried out in a 500 μL volume of 50 mM MES/HEPES buffer containing 30 μM of doxorubicin and varying concentrations of Au nanoparticles (0.4, 0.3 and 0.2 μM) to which 5 mM EDC was added. Conjugation was performed at 30 ºC for 1 h and the conjugates were separated from unconjugated doxorubicin and gold nanoparticles by dialysis. The purified sample collected in the centrifuge tube containing the conjugates were further characterized by UV-Vis and fluorescence spectroscopy, TEM and used further.

For labeling, the HEK293T cells were cultured in high-glucose DMEM (Invitrogen Canada, Burlington, ON) supplemented with L-glutamine (0.2 mM), penicillin (100 U/mL), streptomycin (100 μg/mL), FBS (10%), and incubated in a 5% CO_2 humidified atmosphere (Thermo Electron Corporation, Marietta, OH). We used the cells during the 24-72 hr before use. Conjugates were added to a final concentration of 10 nM gold particles and incubated for 1 hr, then washed three times with PBS and observed. Control cells were incubated with 30 μM doxorubicin alone under the same conditions. Imaging was performed on a Olympus IX70 inverted fluorescence microscope equipped with a Nuance multispectral imaging system (including a visible liquid-crystal filter tunable between 420 and 750 nm) (Cambribge

Research Instruments) Epifluorescence illumination was through a quantum dot filter cube set (excitation=380–460 nm, dichroic 475 nm, emission=500 longpass (LP); Chroma filter 32013). Confocal microscopy was performed on cells after fixation for 30 min in 3.7 % paraformaldehyde. Images were recorded on a Zeiss LSM 510 confocal laser scanning microscope using a PlanApo 100x objective. Simultaneous reflectance and fluorescence channels were used for all images; the fluorescent channel was an Ar laser line (488 nm) and 560 LP emission filter. Reflectance was obtained with a HeNe laser (543 nm) and a 535-590 bandpass output filter.

MTT Assay: Actively growing HEK293 cells were seeded at a density of 5 x 10^3 per well in a 96 well tissue culture plate. The cells were grown till 80% confluency, washed carefully with PBS and incubated with different concentrations of Dox alone (1.5, 2.25, 3 μM) and the Gold-Dox conjugates (20, 30, 40 nM Gold : 1.5 2.25, 3 μM Dox) for 1 h. Each treatment was given in octuplet and assay for each time point was repeated 3 times to ensure reproducibility. After the exposure time the cells were rinsed carefully once with PBS, 200 μl of supplemented DMEM was added and incubated at 37 °C for 18-24 h. After which the reagent (3-(4,5-dimethylthiazol-2-yl)-2,5-diphenyl tetrazolium bromide) (MTT) (12.5 μl from 4 mg/mL) was added into each well and the cells were incubated for 4 h, the cells were rinsed carefully with PBS and 200 μl of dimethylsulfoxide (DMSO) was added into each well. To check mitochondrial dehydrogenase activity, where the MTT is converted to purple-colored formazan. The amount of formazan produced corresponds to the mitochondrial activity of the cells present in each well, which was measured by taking the absorbance at 560 nm on a UV-visible plate reader (Spectra Max Plus, Molecular Devices, Novato, CA). Percent mitochondrial activities of the treated cells against untreated controls were calculated and average mitochondrial activity was represented along with the standard deviation.

UV-Vis absorbance was performed on a Spectra Max Plus plate reader (Molecular devices, Novato, CA) operated at a resolution of 1 nm. Dynamic light scattering measurements were performed on a Zetasizer 5000 (Malvern Instruments) equipped with a He-Ne laser (633 nm, 5 mW), a photomultiplier detector and a Malvern 7132 Multibit autocorrelator. For X-ray diffraction (XRD), films of gold nanoparticles were prepared on Si (111) substrates by drop-coating. XRD was performed on the films with a Discover D8 X-ray diffractometer with a Xe/Ar gas filled Hi-Star area detector and a XYZ platform, operated at 40 kV and a current of 40 mA with Cu Kα radiation. A laser video system was used to optically align the sample with the incident XRD beam. Samples for TEM were prepared on a carbon coated copper TEM grids. TEM measurements were performed on a JEOL Model 2100F EX transmission electron microscope operated at an accelerating voltage of 200 kV. For AFM, samples were prepared by spreading the nanoparticle solution onto a freshly cleaved mica (Grade II) substrate and the solvent was dried using a nitrogen stream. AFM in the intermittent contact mode was performed using an Enviroscope Scanning Probe Microscope equipped with a Nanoscope III A controller from VEECO Digital Instruments, Santa Barbara, CA. AFM tips used were model Arrow-NCR etched Si tip at a resonance frequency of ~300 kHz.

3. Results and discussion

It has been shown previously that microscopic fungi can generate extracellular Au nanoparticles by a process involving NADH-reductases [15]-[16] secreted by the cells under metal stress. We found that when aqueous chloroauric acid was added to an actively growing culture of the fungus *Helminthosporum solani*, the medium turned from colorless to ruby red over a time course of 72 h.

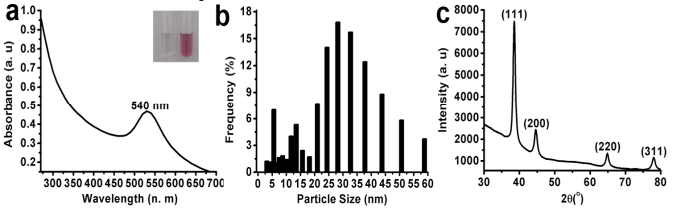

Figure 1. UV-Vis spectra, dynamic light-scattering measurements and XRD of gold nanoparticles formed by the reaction of AuCl4-with fungal biomass. a) UV-Vis spectra recorded from the external medium after 72 h. The inset shows test tubes containing the reaction mixture before (tube on the left, time 0) and after formation of gold nanoparticles (tube on the right, 72 h). b) Dynamic light-scattering particle-size histogram of the solution after 72 h. c) XRD analysis of the gold nanoparticles on a Si (111) wafer. The principal Bragg reflections are identified.

Ultraviolet-visible spectra showed the presence of a surface plasmon resonance (SPR) band centered at 540 nm as shown in figure 1(a) suggesting the presence of Au nanoparticles. Figure 1(b) shows the dynamic light-scattering (DLS) measurements of the mixture indicated the presence of particles in the size range from 3-70 nm. X-ray diffraction (XRD) analysis of a droplet of the mixture on a silica substrate showed intense peaks at (111), (200), (220) and (311) Bragg reflections in the 2θ range 30°-80° as shown in figure 1(c); these agree with values reported for gold nanocrystals [17].

Transmission electron microscopy (TEM) images showed a large number of polydisperse particles as shown in figure 2(a).

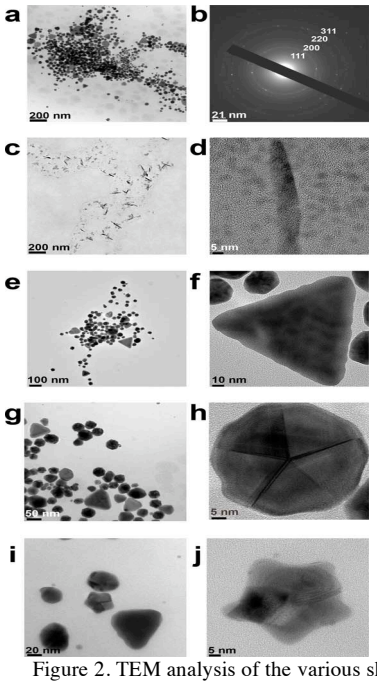

Figure 2. TEM analysis of the various shapes of gold nanoparticles formed after the reaction of AuCl4-with fungal biomass. All images were taken before separation. a) Mixture of all. b) SAED pattern from one of the particles in (a). c) Rod- shaped particles. d) Higher magnification image of one of the rods. e) Triangular particles. f) Higher magnification image of one of the triangles. g) Hexagonal particles. h) Higher magnification image of one of the hexagons. i) Star shaped particles. j) Higher magnification image of one of the stars.

The selected-area electron diffraction (SAED) pattern showed that the particles were crystalline in nature (figure 2(b)). The hexagonal nature of the diffraction spots indicated that the particles were highly oriented (111) with the top normal to the electron beam. The spots could be indexed based on the face-centered-cubic (f.c.c.) structure of gold.

Closer inspection of the particle morphology revealed rods (figure 2(c, d)), triangles (figure 2(e, f)), hexagons (figure 2(g, h)) and stars (figure 2(i, j)). Among 350 particles from a single TEM image, 44% were spherical, 30% triangular, 12% rod-shaped, 7 % hexagonal, 5% pyramidal, and 2 % star-shaped. While the spherical particles were polydisperse in the size range from 2-70 nm, the other shapes were fairly heterogeneous: the rods averaged 13 ± 1 nm long and 7 ± 1 nm wide (n= 39, range 12 nm to 15 nm), the hexagons 36 ± 5 nm in diameter (n= 36, range 30 nm to 42 nm), and the triangles 33 ± 6 nm on a side (n= 45, range 25 nm to 40 nm). The triangular particles were equilateral, flat and with truncated vertices, features generally observed for triangular silver [14] and gold nanoprisms [19] made by chemical/photochemical methods.

Atomic force microscopy (AFM) showed well-dispersed, heterogeneously-shaped nanoparticles (figure 3(a)) with thickness ranging from 2-70 nm (figure 3(b)).

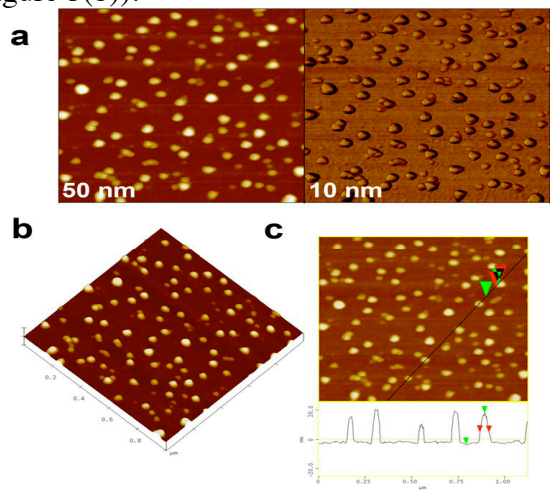

Figure 3. AFM images of the gold nanoparticles. a) Topographical image. b) 3-dimensional view. c) Surface height and length profile of a selected set (black line) of the triangular nanoparticles seen in (b). The arrows indicate the precise points of the profile for a selected particle whose parameters are given in the text.

The surface plot of one of the triangular nanoparticles showed that it had a surface distance of 35.8 nm and vertical distance of 0. 224 nm (figure 3(c)). The surface plot of a pentagon was also carried out on all five edges; the particle had an average surface distance of 41 nm and edge length of 0.307 nm. The particles dispersed well on the mica surface, demonstrating a hydrophilic surface coat.

We were able to separate the nanoparticles based on their size and shape by a density gradient of 30% to

70% sucrose. Fractions of 2 mL were collected and monitored for separation by TEM as shown in figure 4.

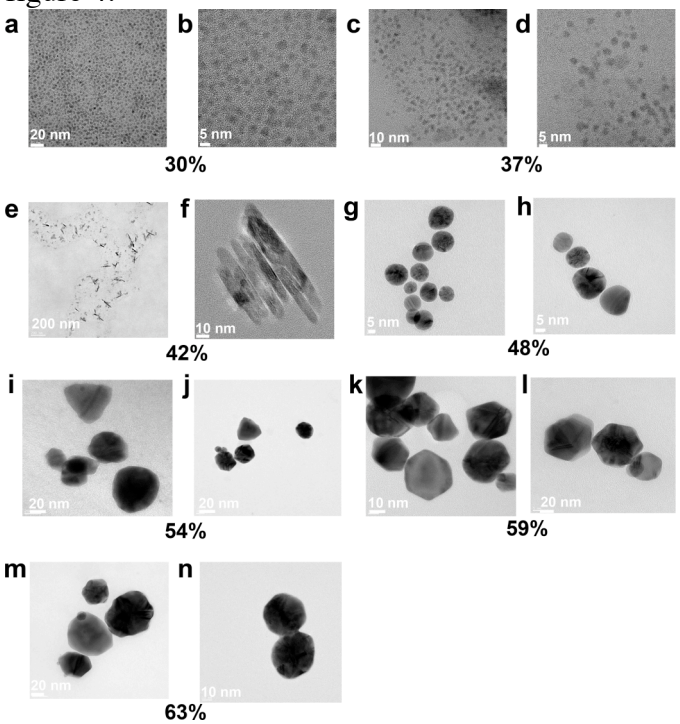

Figure 4. TEM images obtained from different fractions (2 mL) collected after sucrose density gradient of the mixture of gold nanoparticles. a, b) fraction number 1, at 30% (spherical particles between 2-5 nm). c, d) fraction number 7, at 37% (spherical particles between 5-11 nm). e, f) fraction number 12, at 42% (rods, 12-15 nm long and 7-8 nm wide). g, h) fraction number 18, at 48%(spherical particles between the size 14-20 nm). i, j) fraction number 24, at 54% (spherical and triangular particles between 20-35 nm). k, l) fraction number 29, at 59% (hexagonal particles between 30-40 nm). m, n) fraction number 33, at 63% (spherical particles between 50-70 nm).

Spheres from 2-5 nm concentrated in the 30% fraction (figure 4(a, b)); spheres from 5-11 nm in the 37% fraction (figure 4(c, d)); rods in the 42% fraction (figure 4(e, f)); spheres from 14-20 nm in 48% (figure 4(g, h)); spheres and triangles from 20-35 nm in 54% (figure 4(i, j)); pentagons (30-40 nm) in 59% (figure 4(k, l)); and the largest spheres (50-70 nm) in 63% (figure 4(m, n)). In comparison with other separation techniques such as centrifugation, capillary electrophoresis [18], electrophoresis [10], chromatography [13], diafiltration [27], sucrose density gradient separation is advantageous as it is simpler, easier to carry out, and takes less time.

Conjugation of the particles to doxorubicin led to a significant decrease in the absorbance and fluorescence emission of the drug (figure 5(a,c)). It was noticed that there was a shift in the absorbance of the Au SPR in the conjugates (as seen in figure 5b) that might be due to the formation of Au-Dox aggregates which is more prominent upon the dialysis of the conjugates as seen in figure b and d ; however, TEM analysis revealed that the particles remained well-dispersed (figure 5(c-e)).

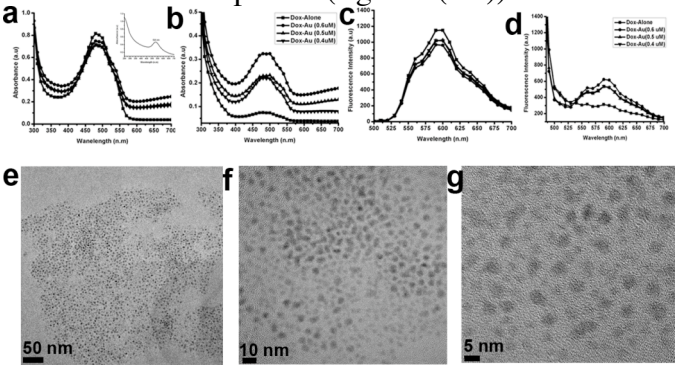

Figure 5. Characterization of Au-doxorubicin conjugates. a) UV-Vis spectra of Au nanoparticles (concentrations 0.4, 0.3 and 0.2 μM) exposed to 30 μM doxorubicin without conjugation or cleaning to establish effect on spectrum. Spectra obtained from conjugates after dialysis (c). Fluorescence emission spectra of the samples in upon excitation at 450 nm, before dialysis (c), after dialysis (d). TEM images of the conjugates at increasing magnification showing excellent dispersity (e-g).

The particles appeared bright under reflectance microscopy at 543 nm; the conjugates alone could also be visualized by reflectance, although they were more readily observed under fluorescence in the doxorubicin channel. The labeling pattern of Au-Dox in HEK293 cells was very different from that seen with dox alone. The drug alone primary concentrates in the nucleus, where it is red, with some green seen outside the cell due to the dependence of the fluorescence on pH and dielectric constant of the medium {Karukstis, 1998 #64} (figure 6 (a)).

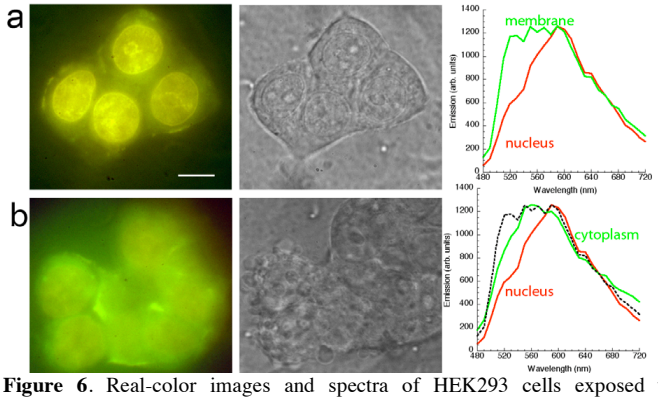

Figure 6. Real-color images and spectra of HEK293 cells exposed to doxorubicin alone (a) and Audoxorubicin (b). Scale bar = 10 !m for all panels. The cells were excited at 400-450 nm and spectra taken from 480-720 nm in 10 nm increments; all spectra are normalized in the graphs, but the visible images were taken under comparable conditions. In (a), most fluorescence appears in the nucleus, and cells under phase contrast appear smooth-edged and healthy. The nucleus shows a broad red fluorescence (peak at 600 nm) whereas the small amount of membrane-associated fluorescence has a green-shifted component. In (b), the cells appear more uniformly bright, and phase-contrast imaging reveals membrane damage in the form of blebbing. The

cytoplasmic fluorescence is greener than that of the nucleus, but less broad than that of membrane-associated dox alone (shown as dashed line).

In contrast, Au-Dox was not seen to enter the nucleus and showed bright fluorescence throughout the cytoplasm that was intermediate in spectrum between the red and green signals seen with dox alone (figure 6(b)). Evidence of oxidative damage in the form of membrane blebbing was seen with Au-Dox but not dox alone (figure 6). Assimilated Au particles could be observed with reflectance and fluorescence confocal microscopy (fig. 7), which further reinforced the differences between the doxorubicin alone and Au-dox labeling. Dox alone concentrated in the cell nucleus, while Au-dox was essentially excluded from the nucleus and appeared to be associated with intracellular membranous organelles (fig. 7 (a, b)). Lysosomal areas of Au-dox cells showed much greater dox fluorescence than Au particle scattering, suggesting that dox may be liberated from the particles in these organelles (fig. 7 (c)).

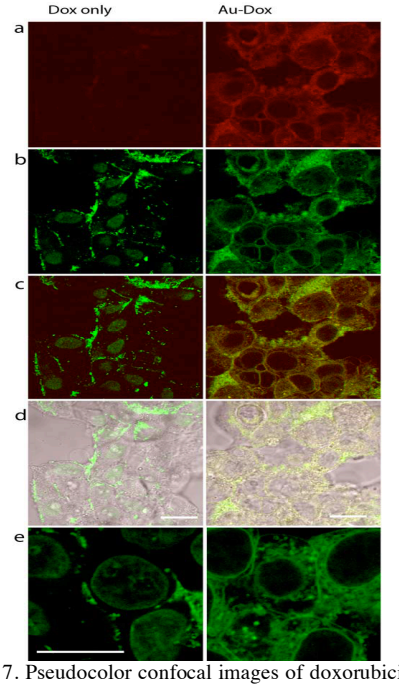

Figure 7. Pseudocolor confocal images of doxorubicin alone (Dox) and Au-doxorubicin in HEK293 cells. Scale bar = 10 !m for all panels. (a) The reflectance image is shown in the red channel, showing little scattering from control cells under these conditions. (b) Doxorubicin fluorescence (560 nm longpass) is shown in the green channel. Note the increased brightness in the Au-Dox cells. (c) Overlay of the red and green channels. (d) Overlay of the red and green channels and d.i.c. image. (e) Higher magnification image showing detail of nuclear labeling in control cells and cytoplasmic labeling in Audox cells.

Brightfield (7(d)) and high power (7(e)) images confirmed these patterns.

On the basis of our repeated experiments, we have selected different concentrations of gold-Dox conjugates for the cytotoxicity and assessed the the effect of the conjugates on cellular metabolic activity using the MTT assay. Enhanced toxicity of doxorubicin upon conjugation to gold nanoparticles was observed, the decrease in the metabolic activity of HEK293T cells treated with the gold-Dox solution determined after 1 h exposure is presented in Figure 8. Untreated cells served as controls and doxorubicin alone was used as a negative control.

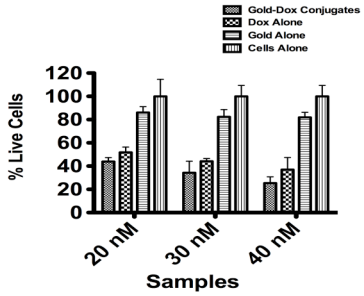

Figure 8. Decrease in the metabolic activity of HEK 293 T cells treated with increasing concentrations of gold=Dox conjugares, and controls as measured by MTT assay.

4. Conclusion

Living cells are the best examples of machines that operate at the nanoscale, performing functions ranging from generation of energy to extraction of targeted materials with very high efficiency. Here we set out to explore the feasibility of synthesizing and separating morphologically diverse Au nanoparticles using methods that are more eco-friendly, simpler and more energy-conserving than chemical synthesis. This is an important step toward the use of these diverse shapes in many biological applications and devices, especially wet devices where the hydrophilic surface coat of the particles will be an asset. The detailed mechanism for the formation of a multi-shaped nanocrystals, and the precise makeup of the protein coat, are currently being investigated. This will allow for purification of the enzymes responsible for the synthesis and thus the development of cell-free synthesis methods that will lend themselves to large-scale production of particles without hazardous chemical waste. It may also permit the controlled synthesis of specific sizes and/or shapes, obviating the need for purification.

In comparison with other separation techniques such as centrifugation, capillary electrophoresis

[18], electrophoresis [10], chromatography [13], diafiltration [27], sucrose density gradient separation is advantageous as it is simpler, easier to carry out, and takes less time. The resulting particles are hydrophilic and show little aggregation, even when conjugated to somewhat hydrophobic molecules such as doxorubicin.

Preliminary experiments with cellular uptake reveal efficient assimilation of Au-doxorubicin conjugates prepared by this method. The conjugates remain cytoplasmic, which may be a desirable feature for maximizing the cytotoxicity of anti-cancer formulations. The fluorescence is also brighter than that seen with comparable concentrations of free dox, probably due to doxorubicin self-quenching, which is also a useful feature for in vivo use. The cytotoxic properties of the gold-Dox conjugates was determined based on cellular metabolic activity, that revealed decrease 10-20% in the metabolic activity of HEK239T cells as compare to doxorubicin alone, allowing their potential usefulness as anti-cancer agents.

Acknowledgements

We thank Mr. Thierry Maris and Mr. Jean-Philippe Masse for assistance in doing XRD and TEM respectively at École Polytechnique de Montreal, Montreal, Canada, and Patricia Moraille for doing AFM at the Laboratoire de caractérisation, Université de Montréal, Montréal, Canada. We also thank Samuel Clarke for helping in making the figures for the manuscript. This work was supported by NSERC Strategic Grant 336830 2006.

References

[1] Alivisatos A P 1996 Perspectives on the physical chemistry of semiconductor nanocrystals *Journal of Physical Chemistry* **100** 13226-39

[2] Bhattacharya D and Gupta R K 2005 Nanotechnology and potential of microorganisms *Critical Reviews in Biotechnology* **25** 199-204

[3] Brown S, Sarikaya M and Johnson E 2000 A genetic analysis of crystal growth *Journal of Molecular Biology* **299** 725-35

[4] Chen S H and Carroll D L 2002 Synthesis and characterization of truncated triangular silver nanoplates *Nano Letters* **2** 1003-7

[5] Courty A, Henry A I, Goubet N and Pileni M P 2007 Large triangular single crystals formed by mild annealing of self-organized silver nanocrystals *Nature Materials* **6** 900-7

[6] Dameron C T, Reese R N, Mehra R K, Kortan A R, Carroll P J, Steigerwald M L, Brus L E and Winge D R 1989 Biosynthesis of Cadmium-Sulfide Quantum Semiconductor Crystallites *Nature* **338** 596-7

[7] El-Sayed M A 2001 Some interesting properties of metals confined in time and nanometer space of different shapes *Accounts of Chemical Research* **34** 257-64

[8] Gericke M and Pinches A 2006 Biological synthesis of metal nanoparticles *Hydrometallurgy* **83** 132-40

[9] Gong J, Zhang Z M, Bai H J and Yang G E 2007 Microbiological synthesis of nanophase PbS by Desulfotomaculum sp *Science in China Series E-Technological Sciences* **50** 302-7

[10] Hanauer M, Pierrat S, Zins I, Lotz A and Sonnichsen C 2007 Separation of nanoparticles by gel electrophoresis according to size-and shape *Nano Letters* **7** 2881-5

[11] Hao E C, Kelly K L, Hupp J T and Schatz G C 2002 Synthesis of silver nanodisks using polystyrene mesospheres as templates *Journal of the American Chemical Society* **124** 15182-3

[12] Hardman R 2006 A toxicologic review of quantum dots: Toxicity depends on physicochemical and environmental factors *Environmental Health Perspectives* **114** 165-72

[13] Henglein A 1993 Physicochemical Properties of Small Metal Particles in Solution - Microelectrode Reactions, Chemisorption, Composite Metal Particles, and the Atom-to-Metal Transition *Journal of Physical Chemistry* **97** 5457-71

[14] Jin R C, Cao Y W, Mirkin C A, Kelly K L, Schatz G C and Zheng J G 2001 Photoinduced conversion of silver nanospheres to nanoprisms *Science* **294** 1901-3

[15] Kumar S A, Abyaneh M K, Gosavi S W, Kulkarni S K, Ahmad A and Khan M I 2007 Sulfite reductase-mediated synthesis of gold nanoparticles capped with phytochelatin. pp 191-5

[16] Kumar S A, Abyaneh M K, Gosavi S W, Kulkarni S K, Pasricha R, Ahmad A and Khan M I 2007 Nitrate reductase-mediated synthesis of silver nanoparticles from AgNO3 *Biotechnology Letters* **29** 439-45

[17] Leff D V, Brandt L and Heath J R 1996 Synthesis and characterization of hydrophobic, organically-soluble gold nanocrystals functionalized with primary amines *Langmuir* **12** 4723-30

[18] Liu F K and Wei G T 2004 Adding sodium dodecylsulfate to the running electrolyte enhances the separation of gold nanoparticles by capillary electrophoresis *Analytica Chimica Acta* **510** 77-83

[19] Malikova N, Pastoriza-Santos I, Schierhorn M, Kotov N A and Liz-Marzan L M 2002 Layer-by-layer assembled mixed spherical and planar gold nanoparticles: Control of interparticle interactions *Langmuir* **18** 3694-7

[20] Manna L, Scher E C and Alivisatos A P 2000 Synthesis of soluble and processable rod-, arrow-, teardrop-, and tetrapod-shaped CdSe nanocrystals *Journal of the American Chemical Society* **122** 12700-6

[21] Medintz I L, Uyeda H T, Goldman E R and Mattoussi H 2005 Quantum dot bioconjugates for imaging, labelling and sensing *Nature Materials* **4** 435-46

[22] Peng X G, Manna L, Yang W D, Wickham J, Scher E, Kadavanich A and Alivisatos A P 2000 Shape control of CdSe nanocrystals *Nature* **404** 59-61

[23] Pintoalphandary H, Balland O and Couvreur P 1995 A New Method to Isolate Polyalkylcyanoacrylate Nanoparticle Preparations *Journal of Drug Targeting* **3** 167-9

[24] Shankar S S, Rai A, Ankamwar B, Singh A, Ahmad A and Sastry M 2004 Biological synthesis of triangular gold nanoprisms *Nature Materials* **3** 482-8

[25] Sun Y G, Mayers B and Xia Y N 2003 Transformation of silver nanospheres into nanobelts and triangular nanoplates through a thermal process *Nano Letters* **3** 675-9

[26] Sweeney R Y, Mao C B, Gao X X, Burt J L, Belcher A M, Georgiou G and Iverson B L 2004 Bacterial biosynthesis of cadmium sulfide nanocrystals *Chemistry & Biology* **11** 1553-9

[27] Sweeney S F, Woehrle G H and Hutchison J E 2006 Rapid purification and size separation of gold nanoparticles via diafiltration *Journal of the American Chemical Society* **128** 3190-7

[28] Yin Y and Alivisatos A P 2005 Colloidal nanocrystal synthesis and the organic-inorganic interface *Nature* **437** 664-70